CT-Based Navigation Guidance for Liver Tumor Ablation

Julian Alpers[1,2][†], Christian Hansen[2][‡], Kristina Ringe[3][§] and Christian Rieder[1][¶]

[1]Fraunhofer MEVIS, Bremen, Germany
[2]Faculty of Computer Science University of Magdeburg, Germany
[3]Department of Diagnostic and Interventional Radiology, Hannover Medical School, Germany

Abstract
Image-guided thermal ablation procedures such as microwave ablation (MWA) or radiofrequency ablation (RFA) have become clinically accepted treatment options for liver tumors. The goal of these minimally invasive procedures is the destruction of focal liver malignancies using mostly needle-shaped instruments. Computed tomography (CT) imaging may be used to navigate the applicator to the target position in order to achieve complete tumor ablation. Due to limited image quality and resolution, the treatment target and risk structures may be hardly visible in intra-interventional CT-images, hampering verification of the intended applicator position.
In this work, we propose a navigation guidance method based only on CT images to support the physician with additional information to reach the target position. Therefore, planning information extracted from pre-interventional images is fused with the current intra-interventional image. The visible applicator is extracted semi-automatically from the intra-interventional image. The localization of the needle instrument is used to guide the physician by display of the pathway, projection of anatomical structures, and correction suggestions. In an evaluation, we demonstrate the potential of the proposed method to improve the clinical success rate of complex liver tumor ablations while increasing the accuracy and reducing the number of intra-interventional CT images needed.

CCS Concepts
●*Human-centered computing* → *Scientific visualization;* ●*Computing methodologies* → *Object detection;* ●*Applied computing* → *Health informatics;*

1. Introduction

The development of minimally invasive liver tumor ablation techniques has provided a promising alternative to surgical resection in the last two decades. Patients are treated typically on an outpatient basis under either conscious sedation or general anesthesia. The ablation instrument is, under imaging guidance, introduced through a small incision in the skin and positioned within a tumor in the liver. In the case of radiofrequency ablation (RFA) or microwave ablation (MWA), energy is applied to the needle's active zone, producing heat within the surrounding tissue. The active zone describes the mostly ellipsoid volume of destruction, which arises during induction of the energy. Temperatures $> 50°$C cause immediate cell death and coagulation necrosis of the tissue surrounding the needle. The success of tumor ablation decreases substantially when larger tumors are treated. Recent guidelines recommend against the ablation of tumors > 3 cm as it is difficult to achieve complete thermal

destruction [CDBL10]. This is due to the difficulty of the precisely positioned and overlapping thermal ablations which are necessary to create a composite ablation to completely eradicate a large tumor. Amongst others, these factors include the lack of a treatment plan, poor tumor visualization and inaccurate positioning of ablation probes. Local recurrence rates after thermal ablation reach 55% [LGL*00] for tumors larger than 3 cm.

Beside other image modalities like Ultrasound, CT imaging may be used to plan the optimal needle trajectory immediately before the percutaneous ablation procedure. During the puncture process, the needle is inserted through the patient's skin in order to place the needle tip inside the planned target. Because the treatment target and the needle are obscured inside the body, CT imaging is used to guide the insertion of the needle instrument (see Figure 1). In a sequential workflow, the CT table carrying the patient is moved into the gantry, CT images are acquired, the current placement is controlled by evaluating the visible needle in the CT image, and subsequently, the CT table is moved out of the gantry to forward the needle further. This workflow is repeated until the needle is finally placed in the intended position. High operator experience is needed to perform safe and accurate instrument placement due

---

† julian.alpers@st.ovgu.de
‡ hansen@isg.cs.uni-magdeburg.de
§ ringe.kristina@mh-hannover.de
¶ christian.rieder@mevis.fraunhofer.de

to several reasons. The nature of intra-interventional CT images is that only few slices (3-5) are recorded with low image quality to reduce the radiation dose, and no contrast agent is injected. Thus, the intra-interventional CT images display the needle with more or less strong metal artifacts depending on the material of the needle. Therefore it may be hard to separate soft tissue ,e.g. tumor from healthy tissue. To control the current placement, the physician has to mentally map the risk structures and treatment target from the planning image to the intra-interventional image where the current needle is visible. Typically, only simple ruler tools are available within CT imaging software packages to verify if the needle's trajectory can reach the treatment target. Another difficulty lies within the clinical workflow. Because the physician wears sterile hand-gloves needed for inserting the needles, only limited interaction with the software is possible.

Figure 1: *Photograph of an image-guided MWA: The patient lies on the table in front of the CT and the radiologist is focusing on the intra-interventional images (upper right display) while trying to adjust the needle position.*

In this work, an application supporting CT-based navigation guidance for liver tumor ablations is presented. The application guides the radiologist during puncture of needle-shaped instruments such as MW applicators. The two major contributions of this work are:

- A needle tracking algorithm which allows reconstruction of the current needle position based on intra-interventional CT images even on low image quality and few image slices.
- Using the reconstructed orientation and position of the needle, augmentation of the intra-interventional image with necessary information from the pre-intervention image, projecting risk structures as well as treatment target, and displaying needle axis elongation and correction suggestions.

The goal of our work is to minimize the human bias and reduce the number of acquired CT images during needle-based interventions, without a significant extension of the intervention time. Therefore, the intra-interventional image is imported from the CT

machine using a DICOM node and the necessary information for navigation is displayed with minimal user input.

The outline of this paper is as follows: Section 2 discusses the related work in terms of instrument detection and common navigation guidance. Section 3 describes the necessary preprocessing steps including the planning of the intervention and the detection of the needle instrument. We present a coarse-fine instrument detection method based on morphological and projection-based approaches. In Section 4 we introduce a navigation system which provides information about the current needle orientation and correction possibilities. Section 5 comprises the evaluation and states the results and achievements of the previously described methods and Section 6 concludes the results with a discussion about the introduced system.

2. Related Work

The success of percutaneous tumor ablation procedures depends on a well planned treatment strategy, monitoring of the procedure, and accurate verification of the therapy success. To facilitate a sufficiently large ablation zone, appropriate ablation devices have to be determined and optimal positions considering the target region have to be chosen [ABLJG11]. During the intervention, the planned therapy strategy has to be transferred to the situation in the operating room (OR) and the therapy progress is monitored using imaging. The goal is to achieve complete destruction of all tumor cells without harming vitally important tissue. After the intervention, the treatment success is verified. A successful therapy is assumed if the tumor is completely enclosed by the coagulation necrosis. The therapy failed if residual tumor tissue is detected outside the coagulation necrosis [Per07].

In recent years, many groups have presented software applications to support the planning process [VSG*04, MCH*06, RSW*09, KKMS, KVK*12], but do not address the transfer of the information into the operation room. To support the physician during the intervention, registration methods have been proposed to align the pre-interventional planning data with the intra-interventional data set of the patient's current anatomy [EOT*10]. In addition, robotic systems have been developed in order to accurately steer the needle to the planned position [CMW*06]. Otherwise, to reduce the radiation dose, optical [SKO*03] or electromagnetic [MWLW08] tracking systems may allow for tracking of the needle position in relation to the pre-interventional image data. Nonetheless these systems are not used in common because they are very expensive, the radiologist has to handle additional equipment in the operating room and the accuracy during tracking varies a lot when it comes to deformable tissue like the liver. Regarding the optical tracking Martelli et al. [MZB*07] provide mostly a text-based visualization for navigation guidance during knee laxity to give a hint about the current angles between the different limbs and the current needle position.

In terms of electromagnetic tracking, Fried et al. [FKG*] started to support the physician during endoscopic surgery using the well-known ortho views of the planning data. In addition, they introduce a special endoscopic view to tprovide information about the current position and view regarding the endoscope. Wood et al. [WZD*05]

performed a feasibility study with different image modalities used for navigation guidance (MR, CT, PET). They introduced a graphical system, which displays triplanar and volumetric views with the possibility to co-display other image modalities for a better navigation support of the physician during needle-based interventions. In the same year, Banovac et al. [BTX*05] presented a non-conventional real-time imaging approach. Their system offers the user an off-axial cross sectional image including the current needle. In addition, they provide depth information through a special depth insertion window and a cross hair targeting window for needle placement support.

In addition, augmented reality approaches have already been proposed to guide the physician during intervention. Sauer et al. [SSK*03] use a head-mounted display (HMD) for the physician to wear. This HMD is used to display virtual models of anatomical targets as an overlay on the patient's skin without any jitter or swimming of the overlay. Due to stereo and kinetic depth cues they even achieve good depth perception. Fichtinger et al. [FDF*05] and Khan et al. [KDM*06] used a mirror-overlay setup. Here, the overlay is projected onto a semi-transparent mirror while the physician is manipulating the needle behind the mirror. Through the mirror, the overlay seems to be floating inside or on top of the patient's body providing good spatial information to the physician. Widmann et al. [WHP*09] tried to transfer the planning data of the intervention into the operating room. They fuse the intra-interventional images with the anatomical planning data to provide information about the spatial relation of their current needle with respect to the planned trajectory path. Ren et al. [RCNY*14] proposed another approach for the transfer of the planning data. They offer several visualizations regarding the planning of the intervention, e.g. semi-transparent overlays for simulated and overlapping ablation zones as well as segmented structures such as tumors and ribs. During intervention, they project their current needle trajectory and the planned trajectory onto the different anatomical views. Chan and Heng [CH14] compared several visualization techniques like lines, strips and ghost meshes regarding the perception of a tilted needle in various directions. In addition, they introduced a new visualization method using a volumetric beam to provide depth information combined with a set of halos to offer information about the orientation and tilting. An overview of computer-assisted planning, intervention, and assessment of liver tumor ablation can be found in [SRB*10].

The detection of surgical tools inside of medical image data via image processing methods is a widely-spread topic regarding minimally invasive interventions. The most common image modality in terms of instrument detection is 3D-US. Here, the different approaches reach from projection-based methods [DWG*06, AAMF09] which reduce the complexity from 3D to 2D, to Hough and Radon transforms [QYD*13, BUM*08] which detect linear objects in images using the corresponding frequency space to find the maximum global function value. Additional work has been proposed regarding the use of Gabor wavelet filters [PZM*15] which aims to model the perceptual neurons of the human brain and the motion displacement analysis [BSRN16] via a vector field analysis of the pre- and intra-interventional datasets. Furthermore, the use of model fitting approaches using of the Random Sample Consensus (RANSAC) algorithm has been introduced by Uherčík et

al. [UKLC10] which tries to fit a model to a set of samples including outliers and large measurement errors.

3. Preprocessing

In this section, the therapy planning before the procedure as well as the required instrument detection, which reconstructs the needle from the pre-interventional image, is presented.
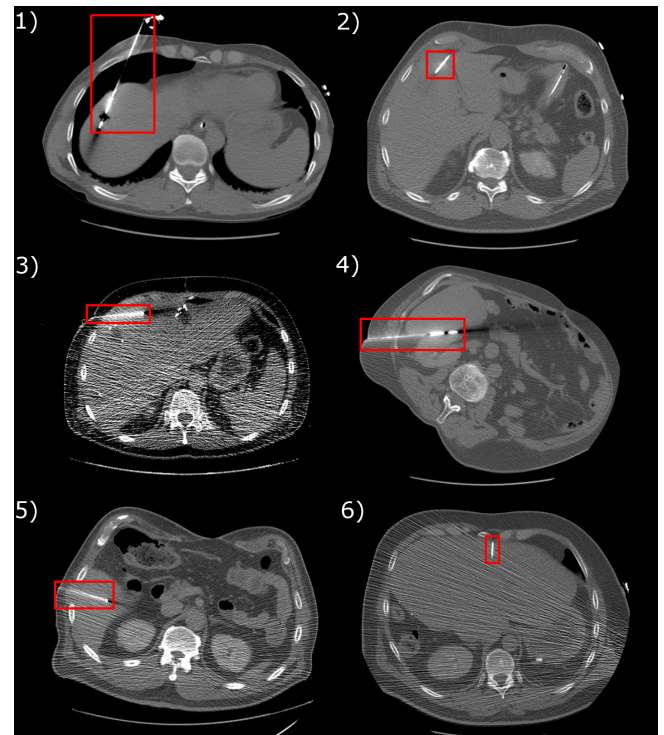
3.1. Therapy Planning

Figure 2: *Intra-operative CT images from different patients containing the needle artifact in various angulations. 1) - 3) RF ablation. 4) - 6) MW ablation.*

Immediately before the intervention, we assume that a full CT scan is acquired in order to plan the procedure. Thereafter, this image is loaded into the planning application either via file system or PACS connection using DICOM nodes. A therapy which relates to the initial planning DICOM image, and thus to a DICOM series, study, and patient is created. Based on the DICOM data, several therapy objects, i.e. instruments or segmentations, can be created per patient. The target tumor as well as risk structures such as vessels can be extracted using semi-automatic segmentation methods and are visualized on top of the anatomical image data. To determine an optimal access path to the target, various virtual instrument models, such as RFA electrodes or MWA antennas, from several vendors can be placed either manually or fully automatic in the viewers. The location and orientation of an instrument can be determined by defining the position of the center of the instrument's active zone (*target point*), and the point of incision (*skin entry point*).

When the intervention starts, intra-interventional CT images showing the needles are acquired. These images are also loaded into the planning application. Therefore, the images are imported via DICOM node and are directly displayed in the software. Optionally, the intra-interventional image can be overlaid with the planning image. If the patient is re-positioned or the target organ moves due to respiration, the intra-interventional image has to be co-registered with the planning image.
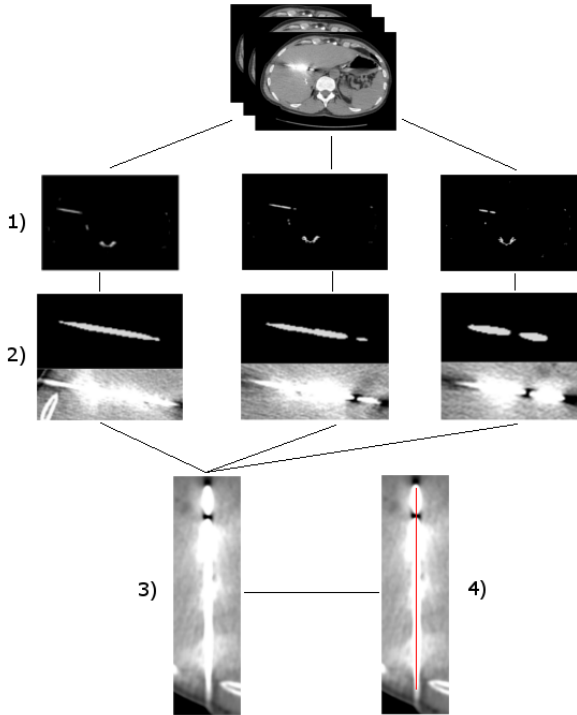
3.2. Instrument Detection

Figure 3: *Image processing pipeline for the instrument detection starting with the original intra-interventional volume followed by the different steps without manual correction. 1) Background removal. 2) Rough needle segmentation. 3) MPR. 4) Final result including the found axis overlaying on the MPR in red.*

Intra-interventional CT images usually consist of only three to five slices. Due to the small size of the image volumes, it is difficult to distinguish the surgical instrument (like a needle) from other structures such as bones, catheters or implants, especially if the needle is not placed in-plane but angulated. Therefore, existing methods like the Radon transform or Hough transform, to detect linear objects in images, are not well-suited to the task. After computation of the Radon- or Hough transform the corresponding frequency space shows the function values for each point in the image. Since the shape of the needle may look like other structures, the global maxima in the frequency space are not obviously correlated to one structure or another, which is why these methods are not suitable for our problem. Nonetheless, robust and accurate detection of the needle instrument is crucial for a proper image-based

navigation guidance system. Therefore, we propose a new instrument detection method on intra-interventional CT images, which includes a simple preprocessing followed by a rough needle axis approximation using a connected component analysis. The final computation of the two endpoints defining the needle's orientation is done using two Multi-Planar Reformations (MPR) in combination with a point shifting based on a histogram analysis. Note that in the following, the term "tip of the needle" refers to the center of the active zone and the term "shaft of the needle" refers to the skin entry point. An overview about our method can be observed in Figure 3. After importing, the images need to be normalized according to the intercept, slope, and data values depending on the individual CT scanner. The normalized image is filtered using a Gaussian filter with $\sigma = 1$ to reduce noise and remove slight artifacts caused by the needle. Additionally, the blurring effect causes the needle to appear slightly thicker than before. This behavior is valuable because it supports the subsequent morphological closing, which is performed in a later step using a 3x3 kernel to close holes in the segmentation caused by the energy emitting point within the tip of the needle. The detection of the actual needle is performed using the following five steps:

Step 1 The background of the image has to be removed using the standardized Hounsfield Units (HU). The threshold is set to 300 HU to make sure that the soft tissue is removed safely. Only a few structures are typically left over, including the needle and parts of the spine and the ribs. Additionally, include and exclude masks can be used to increase the success rate of finding the needle while decreasing the computational time. These masks can be the patient's skin mask or the segmentation mask of the bones, for example. They may be already present outside of the preprocessing steps, e.g. due to the automatic instrument placement or registration methods).

Step 2 The remaining structures are clustered using a connected component analysis. The resulting objects are filtered according to their size, removing all clusters with a volume greater than 10,000 voxels and lower than 30 voxels, which correlates to the observed min and max volumes of the needle artifacts. This wide range originates from the various needle angulations, which may occur during intervention (see Figure 2). The filtering according to the cluster size causes the spine to be removed as well as several outliers and artifacts. Using the remaining set of objects, a shape ratio is computed for every object. This ratio sets the longest extent L in contrast to the medium M and shortest S extent of the object using the following formula with i as the index of the current object:

$$R_i = \frac{L_i}{M_i + S_i} \tag{1}$$

This shape ratio presents a higher value for elongated objects. Clinical observation shows that the trajectory path of the inserted needle is mostly in-plane, which is why the needle is visible as an elongated artifact most of the time and therefore the shape ratio is suitable.

Step 3 After finding the object which corresponds to the needle, the exact needle axis is refined. Therefore, we take the longest axis of the object as an initial input for an MPR along this axis. This results in a projection of the 3D image onto a 2D plane (see Figure

4). To ease the following tasks, the image is rotated in such a way that the previously defined axis is orientated parallel to the y-axis of the corresponding coordinate system. Using this projection, we perform a horizontal histogram analysis parallel to the x-axis in a defined window of 50mm. This window is defined as the doubled size of the maximal observed needle diameter regarding a database covering various needles of different type and from different vendors. We assume that the original needle axis corresponds to the highest intensity values within the needle artifact. Thus, the endpoint is shifted to the corresponding intensity maximum along the horizontal intensity profile. Afterwards, the image is rotated again with the result that the new axis is once more parallel aligned to the y-axis. The second histogram analysis is performed vertically to find the strongest gradient descent as defined by Pourtaherian et al. [PZdW*14]. After shifting the endpoints, the needle axis is back-projected into the corresponding 3D space resulting in the exact needle axis.
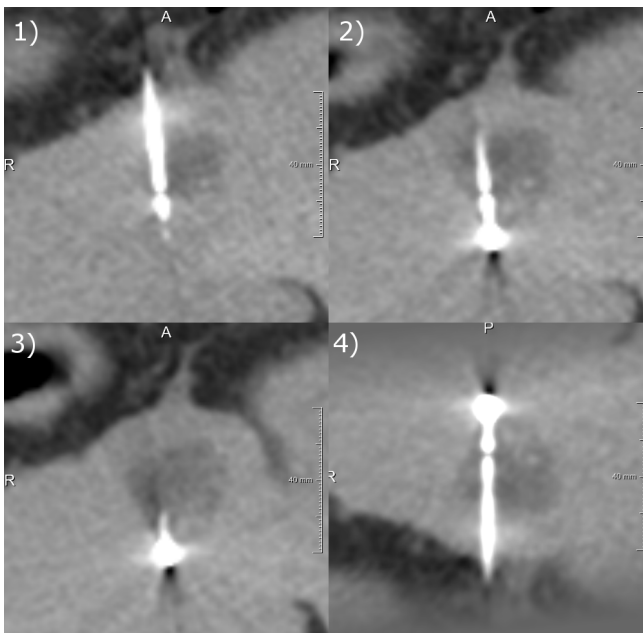

Figure 4: *1)-3) Three individual slices out of the intra-interventional CT scan. 4) Resulting 2D projection after computation of the MPR along the coarse needle axis. The result is rotated in such a way that the needle axis is aligned parallel to the y axis.*

Step 4 In the last small step, the needle axis is elongated to intersect with the patient's skin, because the artifacts may not. Therefore the found needle axis is elongated in direction of the shaft endpoint until it hits the iso-surface of the of the patient skin. The intersection with the iso-surface defines the final position for the shaft endpoint marker.

Step 5 In the case of a false positive detection, i.e. if another structure is mistakenly detected as the needle, the user can manually define a Region of Interest (ROI) by clicking into the surrounding area of the needle. This triggers a re-computation within the ROI

only, which typically takes less than one second. In addition, both endpoints can be moved separately via drag and drop to adjust the position of these points.

4. Navigation Guidance

During needle-based interventions the radiologist has no view into the human body. Thus, landmark structures have to be remembered from the pre-interventional planning image and guess the correct insertion direction of the needle based on this information. This process depends strongly on the operator's experience and is thus prone to human error, which may lead to a significant miscalculation in needle placement and thus incomplete tumor ablation. To overcome this problem, an appropriate visualization for navigation guidance, which projects the planning information onto the intra-operative images, is needed. A good monitoring system should be able to support the radiologist in a more accurate puncture of the needle while taking less time. Also, this would lead to fewer images needing to be acquired, therefore reducing the patient's exposure to radiation. One part of such a system covers the topic of needle detection stated in Section 3.2. The following subsection describes the visualization part of the system.
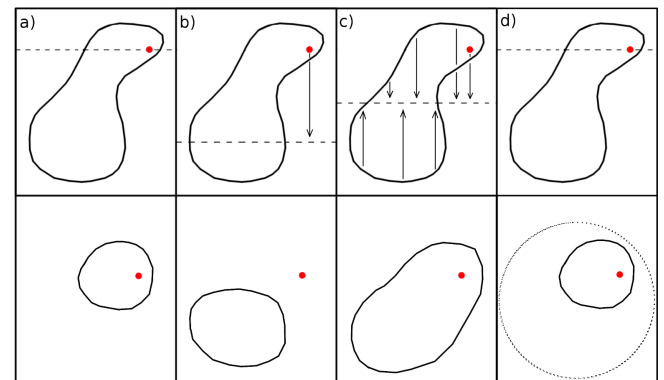
4.1. Target Structure Projection

Figure 5: *Sketch of the four different approaches. Top: Sagittal view at the target structure including needle intersection point. Bottom: Projected outline including needle intersection point. a) Simple axial slicing. b) Axial slicing through the highest global extent. c) Maximum intensity projection. d) Used combined approach.*

The first step in the visualization pipeline covers the projection of the target structure location into the intra-operative image. This location is defined not by the target structure itself, but by the previously planned needle tip position. Therefore, four different approaches for target visualization are discussed in the following.

The first and easiest approach is a simple slicing of the binary mask of the target structure. Here, the planned needle tip position is taken and the axial slice of the target mask around the tip position is outlined. This approach is very simple and intuitive as it does not lead to any visual clutter as it only shows the information which is expected. The main disadvantage of this simple approach is the fact that the resulting visualization only provides the user with the

local extent information of the target structure in the axial slice of the planned target point. On the other hand, the user does not get any information about the global maximum extent of the target structure (e.g. in another axial slice or in depth), meaning that there is no hint if the presented extent is big or small related to the whole structure.

The second approach does not aim for the visualization of the local extent but rather the maximum global extent of the target structure. Therefore the slice with the maximum extent of the target structure is projected onto the intra-operative images as well as the planned tip position. This method is also fast, but it may mislead the radiologist's decision due to the inconsistency of the shown information; the maximum axial extent of the target structure would be stated, but the target location may not correspond to the projected slice. Therefore the radiologist may see that the projected target structure would be hit, but in reality it would be missed the target is of an unusual shape.

The third and most complex approach to visualize the target structure is a Maximum Intensity Projection of the target mask. This would lead to global information about the shape of the target structure in the axial plane. Nonetheless, this approach leads to the same negative effects as stated in the second method, while being more time consuming overall.
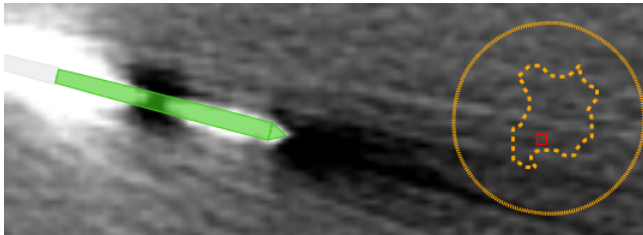

Figure 6: *Projection of the tumor outline (stippled) and the corresponding bounding sphere (fine dotted). The tumor does not intersect the current intra-interventional slice. In addition, the needle object can be seen inside the artifact.*

After comparing all three approaches, we decided to split the information about the local and global extent information. Therefore, the first approach was used to visualize the local tumor extent as outline. In addition, a minimum bounding sphere of the target structure is computed. This bounding sphere defines the smallest possible sphere encompassing the target structure. The diameter of this sphere is also visualized to provide information about the global maximum extent of the structure, as well as the center of mass, which corresponds to the center of the sphere. All approaches, including the final one, are sketched in Figure 5. The resulting projection within the final system can be seen in Figure 6.

4.2. Elongated Trajectory Path

Due to the CT artifacts, the exact trajectory of the needle to the treatment target can not always be robustly defined. The artifacts lead to a detection uncertainty which is represented by a detection error. The error value is defined by computing the average Euclidean distance between the detected needle axis and the centerline

of the segmentation mask. The average distance between these two lines defines the used detection error, which usually lies between 0.5mm and 1.5mm.
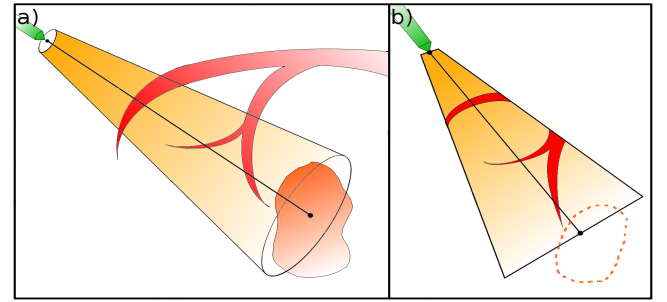

Figure 7: *a) Illustration of the truncated cone and a vessel risk structure as well as the needle and the tumor. b) Sketch of the resulting projection onto the current intra-interventional slice.*

After the definition of an appropriate detection error, the intersection of the tracked needle axis with the target structure needs to be computed. Therefore, a plane is defined using the previously planned target point as location input and the inverse needle axis direction as the surface normal. Taking this into account, the plane can be defined using the point-normal form:

$$\overrightarrow{n} \cdot (\overrightarrow{x} - \overrightarrow{x_0}) = 0. \tag{2}$$

with $\overrightarrow{n}$ as the normal vector of the plane, $\overrightarrow{x_0}$ as the initial point located on the plane and $\overrightarrow{x} = (x, y, z)$ as any point on the plane. The intersection of the elongated needle axis is afterwards computed using plane information and the line equation of the needle axis. The intersection point sI of the line and the plane is then computed as following:

$$sI = \frac{-(ax_0 + by_0 + cz_0 + d)}{(\overrightarrow{n} \cdot \overrightarrow{u})} \tag{3}$$

using $\overrightarrow{n} = (a, b, c)$, (x_0, y_0, z_0) as an initial point on the plane and the normalized direction vector $\overrightarrow{u}$ of the needle axis, which is calculated from the detected skin entry point P_0 and needle tip P_1. Having regard to the detection error, the points P_0 and P_1 are contrary shifted by the amount of the detection error along the perpendicular vector of $\overrightarrow{u}$. This results in a new direction vector $\overrightarrow{u_t}$ which is used to compute a second line-plane intersection point sI_t. The Euclidean distance between the two intersection points defines the maximum error position at the target location (target error), which may occur during intervention. Taking the initial detection error and the target error into account results in a truncated error cone along the elongated needle until the target is hit (see Figure 7. To visualize this information, the truncated cone is projected onto the z-dimension and is displayed as a semi-transparent overlay in the acquired intra-interventional image (see Figure 8).

4.3. Depth Visualization

The core part regarding an intra-operative monitoring system is the appropriate visualization of the depth information. The extents of the structures in the axial view can be observed very well, but since
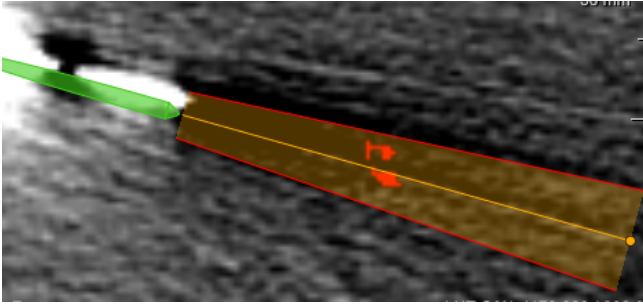
Figure 8: *Projection of the error cone and the corresponding risk structure intersections (red structures inside of the cone). In addition, the needle object can be seen inside the artifact. The radius of the cone right at the tip of the needle corresponds to to the initial detection error.*

Figure 9: *Left: Sketch of the sweep line algorithm. The horizontal stippled line indicates the sweep line passing the different risk structures in z-dimension. Green: Already processed. Yellow: In progress. Red: Not visited yet. Right: Resulting viewport including bar glyphs, which represent the different risk structures (tan bars), the current needle intersection slice (blue line) and the target structure (red bar) including the exact target slice (white line within the bar).*

intra-operative images are restricted to few slices for each volume, the radiologist needs considerable experience to reconstruct the location of his currently acquired images and the related position of the target structures. To address this problem, we implemented a *Depth Scale* to set all relevant structures in relation to each other. The scaling itself has two different modes. It is either scaled to the whole pre-interventional image or restricted to an area that encompasses all relevant structures. The former puts the structures into a global relation to each other in such a way that the single slices correspond to the shown scales. The latter provides a more detailed local information about the relation of the structures.

The target structure is visualized by taking the extent in z-direction and scaling it to one of the previously chosen volume regions. The computation of the corresponding viewport region for each risk structure is done using an adapted form of the sweep line algorithm proposed by Tietjen et al. [TMS*06] (see Figure 9). The resulting box glyphs show their spatial relation among themselves as well as the spatial relation to the previously defined volume of interest, and the target structure.

4.4. Target View

Even though the *Depth Scale* offers good global information about the spatial relation of all structures along the possible needle trajectories, it might be difficult to distinguish between those structures. To overcome those possible ambiguities, the current needle detected from the intra-interventional image is also displayed together with the planned needle, risk structures, and target tumor in a 3D volume rendering of the pre-interventional planning image. Since user interaction is required to explore possible intersections of the needle trajectory with risk structures, we provide a bullseye inspired visualization. The so-called *Target View* displays the complete trajectory from the skin entry point to the target point. If a new needle is detected, the target view is updated automatically. This allows the radiologist to directly see the possible risk structures within the needle path without the need to interact with the rendering.
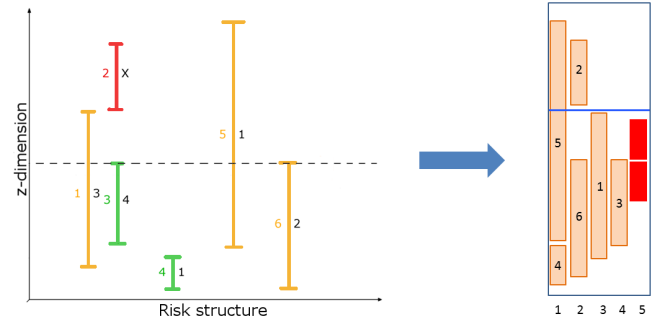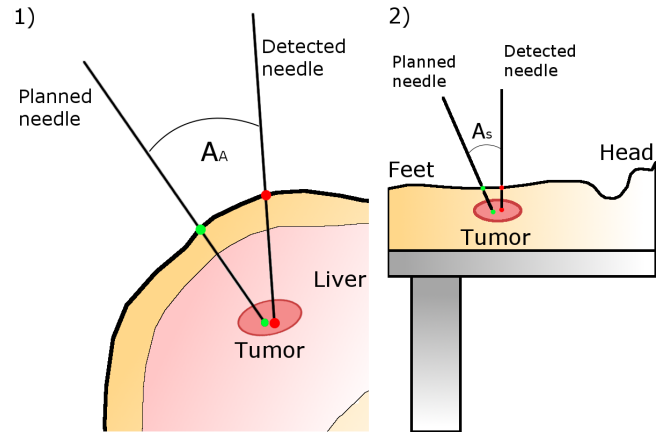

Figure 10: *1) Illustration of the axial correction angle A_A. 2) Illustration of the sagittal correction angle A_S. Both angles are computed separately between the planned and detected trajectory path.*

4.5. Correction Suggestion

The last contribution regarding our intra-interventional visualization is the suggestion of an appropriate correction of the needle placement. Therefore, the difference in the angle between the current intersection point and the planned target point is displayed. For a better and more intuitive translation onto the real needle in the operating room, the angle is divided into the axial and sagittal part. The angles A_A and A_S are computed using the following equations:

$$A_A = \arccos(v_c(x,y) \cdot v_t(x,y)) \tag{4}$$

$$A_S = \arccos(v_c(y,z) \cdot v_t(y,z)) \tag{5}$$

with A_A and A_S defining the axial and sagittal angle and v_c defining the vector between the skin entry point and the current intersection point, whereas v_t defines the vector between the skin entry point

and the target point (see Figure 10). x, y, z correspond to the single components of each vector. The computed angles are color coded based on a threshold which assumes that an appropriate orientation is reached when the angle between the current intersection point and the target point amounts to less than one degree. In this case, a green color indicates that the orientation is quite good. A yellow color assumes an angle between one and five degrees and indicates that the radiologist has to be careful while inserting the needle. A red color coding assumes that the angle amounts to more than 5 degrees in difference and indicates an error which may lead to miss the target structure.

A full implementation of our work can be seen in Figure 13, as well as other parts of the therapy planning software in which it was integrated. The system itself is divided into different views. On the left the image and list views are shown as well as the different components. The viewers on the right display the anatomical planning images in addition to the monitoring system in the upper left corner. This allows us to provide information to the radiologists which they are used to. In addition we provide the possibility to switch to a 3D view if necessary (see Figure 11).
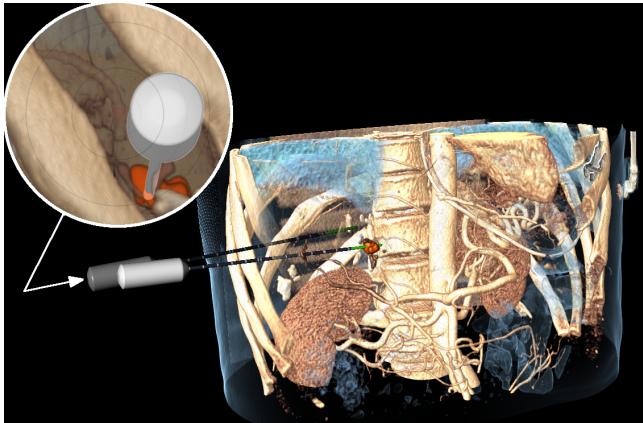

Figure 11: *Volume visualization of a contrast enhanced preinterventional CT image with segmented tumor (orange). The light gray instrument is the planned needle, the dark gray is the needle reconstructed from the current intra-interventional CT image. The target view (upper left) shows the view through the current needle.*

5. Results

An initial evaluation of the proposed needle detection method was performed using 15 intra-operative data sets showing MW ablations of a tumor inside the liver. All computations were made without the use of any other a priori knowledge like the bone mask and no restrictions to a certain region of interest. The test data consisted of 15 three-slice intra-interventional patient CT images, each showing a single MWA needle with different angulations. All computations were performed using an Intel(R) Core(TM)2 Duo CPU E8500 @ 3.16GHz 3.16GHz with 8GB RAM on a 64-bit system. Out of the 15 cases, five were detected correctly without any manual correction, while eight needle detection results had to be corrected using one of the methods stated at the end of Subsection 3.2.

If the needle estimation was not able to find the needle artifact, even with the limitation to a ROI, the detection was classified as a failure. Even in these two failed cases, a manual manipulation of the shaft and tip endpoint markers would have been possible to generate an appropriate input for the navigation guidance. After importing the intra-operative images, the average computation time to detect the needle axis was 3.45 ± 0.2 seconds. Although the goal of this work was not to optimize the performance of the detection algorithm, the clinical expert stated that waiting 3.5 seconds on average will not hamper the clinical workflow.

To evaluate the monitoring system, the clinical workflow was simulated by performing virtual liver punctures. Therefore, an evaluation application consisting of two viewers has been developed. To simulate the intervention, the iso-surface of the patient skin based on the planning image was rendered on the left. It included a virtual needle to perform the simulated interventions by dragging the handle of the instrument with the mouse. On the right, the proposed navigation guidance is presented. The intensity values of those images were windowed in such a way that no soft tissue can be distinguished and the user can only rely on the introduced monitoring system (see Figure 12).
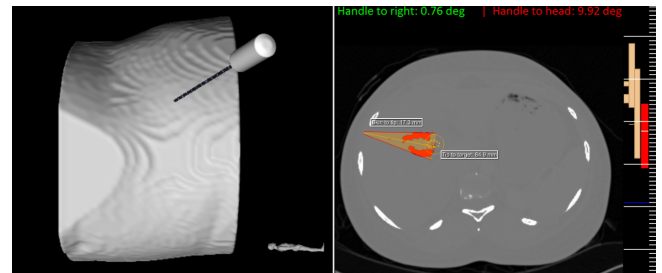

Figure 12: *Left: Virtual patient including an ablation needle. The needle can be moved by dragging the handle and inserted by dragging the shaft. Right: Simulated intra-operative image. Navigation is only possible using the proposed navigation guidance system.*

The simulation was performed by one highly experienced radiologist and one medical technical assistant (MTA) without any experience via manipulation of the virtual needle and the simulation of intra-interventional images. During evaluation, the measured accuracy in relation to the time needed for the intervention as well as the number of simulated intra-operative images acquired are stored for statistical analysis.

The accuracy was defined by computing the Euclidean distance between the previously planned target point and the final tip position of the simulated instrument. The results show that the average error in accuracy was <1.8mm for both experts. In addition, it was observed that the number of simulated intra-interventional images highly correlates with the time needed for one intervention, with an average number of ten images simulated for both experts and 194.76 seconds for the average time needed for the intervention. More detailed results can be observed in Table 1.

In addition to the statistical evaluation, an interview with a highly experienced interventional radiologist was performed. After the presentation of our system, two opinions were clearly stated. On

the one hand, a highly experienced radiologist would not rely on this kind of system when it comes to an easy liver ablation without any axial off-plane angulation of the needle. In this case, a simple measurement tool would be sufficient to plan the trajectory, and during the intervention the needle would always be completely visible, allowing a safe and accurate puncture with some experience. On the other hand, a more complex intervention which forces the radiologist to tilt the needle off-plane may be very challenging even for experienced radiologists. Here, it was stated that a monitoring system would probably be able to aid the performing radiologist during intervention. This kind of system may increase the success rate of more complex liver ablations and therefore contribute to a higher outcome of those interventions, in particular for inexperienced physicians. Apart from these two statements, it was clearly said that in any case it would be very reassuring to have such an intra-interventional system, to verify the current needle position if needed.

Subject	Time [sec]	Acc. [mm]	#Images
MTA	166.05 ± 89.96	1.74 ± 0.79	8.5 ± 3.8
Radiologist	223.47 ± 122.87	1.71 ± 0.89	11.6 ± 5.3

Table 1: *Results of the monitoring system evaluation. Each of the two subjects was evaluated in terms of the time needed for placing the needle (Time [sec]), the accuracy in placement (Acc. [mm]), and the number of simulated intra-operative images (#Images).*

6. Discussion and Conclusion

In this paper, we introduced an application supporting CT-based navigation guidance for liver tumor ablations. As a necessary part of the preprocessing, we described a basic instrument detection method working on intra-interventional CT scans. This approach focuses on projection-based and morphological methods to reduce the computational time as much as possible. Afterwards, the detected instrument axis is used as an input for the monitoring component of our introduced application resulting in a set of visualizations to support the radiologist during needle placement. During all steps, we assume the patient is in a stable breath-hold state and therefore do not consider non-rigid organ movements or deformations. In case a breath-hold state is not achievable, those movements and deformations could be compensated by deformable registration methods. Our system was initially evaluated by two experts through perfection of 15 simulated liver ablation scenarios. Both experts showed accurate results with a placement error of <1.8mm for each case and an average number of simulated intra-interventional images < 12. The separation of the first and second dimension information from the third dimension information was said to be very helpful. In addition, a highly experienced interventional radiologist evaluated the system subjectively, stating that the proposed method would be very reassuring and very helpful during more complex liver ablations with off-plane angulated trajectory paths.

Regarding the instrument detection, it is obvious that much improvement is necessary to reduce the needed interaction as much as possible. With respect to the medical workflow during the intervention, it would be advisable to take more a priori knowledge into account. One example would be the use of the orientation and location of a previously detected instrument axis (or the planned trajectory path) to define a ROI beforehand. Another promising technology may be deep learning.

As future work, a clinical prospective study has to be performed to prove the value of our application. In addition, the realization of our described visualizations, inside the monitoring system, need to be evaluated and discussed in detail to dissolve possible ambiguities. Furthermore, it would be advisable to combine this system with other navigation guidance techniques to allow the radiologist to keep his focus on the patient. Regarding this point, auditory feedback could be considered as additional support [BHN*17].

To conclude this work, our instrument detection offers the potential for more improvement to reduce the needed correction interactions. The monitoring system, as part of our introduced application, shows a high potential to improve the clinical success rate of complex liver tumor ablations while increasing the accuracy and reducing the needed CT images.
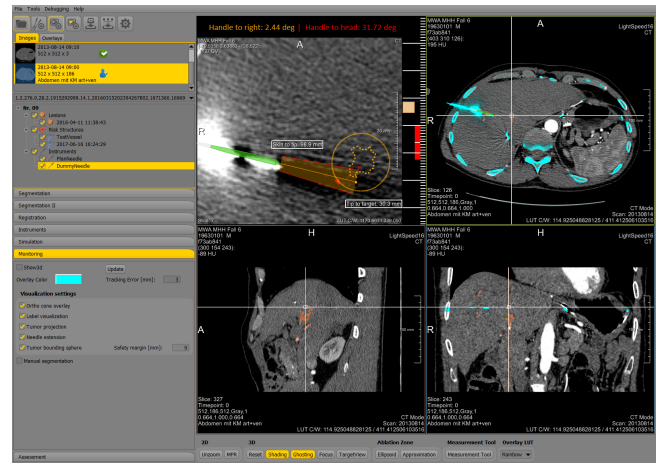

Figure 13: *Screenshot of the planning application showing the monitoring step. An intra-interventional image is loaded which is overlaid on top of the planning image in axial (upper right), sagittal (lower left) and coronal (lower right). The upper left viewer displays the proposed navigation guidance visualizations.*

Acknowledgements

References

[AAMF09] ABOOFAZELI M., ABOLMAESUMI P., MOUSAVI P., FICHTINGER G.: A new scheme for curved needle segmentation in three-dimensional ultrasound images. In *2009 IEEE Int. Symp. on Biomedical Imaging: From Nano to Macro* (2009), pp. 1067–1070. 3

[ABLJG11] AHMED M., BRACE C. L., LEE JR F. T., GOLDBERG S. N.: Principles of and advances in percutaneous ablation. *Radiology 258*, 2 (2011), 351–369. 2

[BHN*17] BLACK D., HANSEN C., NABAVI A., KIKINIS R., HAHN H.: A survey of auditory display in image-guided interventions. *International Journal of Computer Assisted Radiology and Surgery* (2017), 1–12. 9

[BSRN16] BEIGI P., SALCUDEAN S. E., ROHLING R., NG G. C.: Automatic detection of a hand-held needle in ultrasound via phased-based analysis of the tremor motion. In *SPIE Medical Imaging* (2016), International Society for Optics and Photonics, pp. 97860I–97860I. 3

[BTX*05] BANOVAC F., TANG J., XU S., LINDISCH D., CHUNG H. Y., LEVY E. B., CHANG T., MCCULLOUGH M. F., YANIV Z., WOOD B. J., ET AL.: Precision targeting of liver lesions using a novel electromagnetic navigation device in physiologic phantom and swine. *Medical physics 32*, 8 (2005), 2698–2705. 3

[BUM*08] BARVA M., UHERCIK M., MARI J.-M., KYBIC J., DUHAMEL J.-R., LIEBGOTT H., HLAVÁC V., CACHARD C.: Parallel integral projection transform for straight electrode localization in 3-d ultrasound images. *ieee transactions on ultrasonics, ferroelectrics, and frequency control 55*, 7 (2008), 1559–1569. 3

[CDBL10] CROCETTI L., DE BAERE T., LENCIONI R.: Quality improvement guidelines for radiofrequency ablation of liver tumours. *Cardiovascular and interventional radiology 33*, 1 (2010), 11–17. 1

[CH14] CHAN W.-Y., HENG P.-A.: Visualization of needle access pathway and a five-dof evaluation. *IEEE journal of biomedical and health informatics 18*, 2 (2014), 643–653. 3

[CMW*06] CLEARY K., MELZER A., WATSON V., KRONREIF G., STOIANOVICI D.: Interventional robotic systems: Applications and technology state-of-the-art. *Minimally Invasive Therapy & Allied Technologies 15*, 2 (2006), 101–113. 2

[DWG*06] DING M., WEI Z., GARDI L., DOWNEY D. B., FENSTER A.: Needle and seed segmentation in intra-operative 3d ultrasound-guided prostate brachytherapy. *Ultrasonics 44* (2006), e331–e336. 3

[EOT*10] ELHAWARY H., OGURO S., TUNCALI K., MORRISON P. R., TATLI S., SHYN P. B., SILVERMAN S. G., HATA N.: Multimodality non-rigid image registration for planning, targeting and monitoring during ct-guided percutaneous liver tumor cryoablation. *Academic radiology 17*, 11 (2010), 1334–1344. 2

[FDF*05] FICHTINGER G., DEGUET A., FISCHER G., IORDACHITA I., BALOGH E., MASAMUNE K., TAYLOR R. H., FAYAD L. M., DE OLIVEIRA M., ZINREICH S. J.: Image overlay for ct-guided needle insertions. *Computer Aided Surgery 10*, 4 (2005), 241–255. 3

[FKG*] FRIED M. P., KLEEFIELD J., GOPAL H., REARDON E., HO B. T., KUHN F. A.: Image-guided endoscopic surgery: Results of accuracy and performance in a multicenter clinical study using an electromagnetic tracking system. *The Laryngoscope 107*, 5, 594–601. 2

[KDM*06] KHAN M. F., DOGAN S., MAATAOUI A., WESARG S., GURUNG J., ACKERMANN H., SCHIEMANN M., WIMMER-GREINECKER G., VOGL T. J.: Navigation-based needle puncture of a cadaver using a hybrid tracking navigational system. *Investigative radiology 41*, 10 (2006), 713–720. 3

[KKMS] KHLEBNIKOV R., KAINZ B., MUEHL J., SCHMALSTIEG D.: Crepuscular rays for tumor accessibility planning. *IEEE transactions on visualization and computer graphics 17*, 12, 2163–2172. 2

[KVK*12] KERBL B., VOGLREITER P., KHLEBNIKOV R., SCHMALSTIEG D., SEIDER D., MOCHE M., STIEGLER P., PORTUGALLER R. H., KAINZ B.: Intervention planning of hepatocellular carcinoma radio-frequency ablations. In *Workshop on Clinical Image-Based Procedures* (2012), Springer, pp. 9–16. 2

[LGL*00] LIVRAGHI T., GOLDBERG S. N., LAZZARONI S., MELONI F., IERACE T., SOLBIATI L., GAZELLE G. S.: Hepatocellular carcinoma: radio-frequency ablation of medium and large lesions 1. *Radiology 214*, 3 (2000), 761–768. 1

[MCH*06] MCCREEDY E., CHENG R., HEMLER P., VISWANATHAN A., WOOD B., MCAULIFFE M.: Radio frequency ablation registration, segmentation, and fusion tool. *IEEE Trans Inf Technol Biomed 10*, 3 (July 2006), 490–496. 2

[MWLW08] MUNDELEER L., WIKLER D., LELOUP T., WARZÉE N.: Development of a computer assisted system aimed at rfa liver surgery. *Computerized medical imaging and graphics 32*, 7 (2008), 611–621. 2

[MZB*07] MARTELLI S., ZAFFAGNINI S., BIGNOZZI S., LOPOMO N., MARCACCI M.: Description and validation of a navigation system for intra-operative evaluation of knee laxity. *Computer Aided Surgery 12*, 3 (2007), 181–188. 2

[Per07] PEREIRA P. L.: Actual role of radiofrequency ablation of liver metastases. *European radiology 17*, 8 (2007), 2062–2070. 2

[PZdW*14] POURTAHERIAN A., ZINGER S., DE WITH P., KORSTEN H. H., MIHAJLOVIC N.: Gabor-based needle detection and tracking in three-dimensional ultrasound data volumes. In *2014 IEEE International Conference on Image Processing (ICIP)* (2014), pp. 3602–3606. 5

[PZM*15] POURTAHERIAN A., ZINGER S., MIHAJLOVIC N., HUANG J., NG G. C., KORSTEN H. H., ET AL.: Multi-resolution gabor wavelet feature extraction for needle detection in 3d ultrasound. In *Eighth International Conference on Machine Vision* (2015), International Society for Optics and Photonics, pp. 987513–987513. 3

[QYD*13] QIU W., YUCHI M., DING M., TESSIER D., FENSTER A.: Needle segmentation using 3d hough transform in 3d trus guided prostate transperineal therapy. *Medical physics 40*, 4 (2013), 042902. 3

[RCNY*14] REN H., CAMPOS-NANEZ E., YANIV Z., BANOVAC F., ABELEDO H., HATA N., CLEARY K.: Treatment planning and image guidance for radiofrequency ablation of large tumors. *IEEE journal of biomedical and health informatics 18*, 3 (2014), 920–928. 3

[RSW*09] RIEDER C., SCHWIER M., WEIHUSEN A., ZIDOWITZ S., PEITGEN H.-O.: Visualization of risk structures for interactive planning of image guided radiofrequency ablation of liver tumors. In *Procedings SPIE* (2009), p. 726134–726134. 2

[SKO*03] SEQUEIROS R. B., KLEMOLA R., OJALA R., JYRKINEN L., VAARA T., TERVONEN O.: Percutaneous mr-guided discography in a low-field system using optical instrument tracking: A feasibility study. *Journal of Magnetic Resonance Imaging 17*, 2 (2003), 214–219. 2

[SRB*10] SCHUMANN C., RIEDER C., BIEBERSTEIN J., WEIHUSEN A., ZIDOWITZ S., MOLTZ J.-H., PREUSSER T.: State of the art in computer-assisted planning, intervention and assessment of liver tumor ablation. *Critical Reviews^{TM} in Biomedical Engineering (Special Issue on Thermal Tumor Ablation) 38*, 1 (2010), 31–52. 3

[SSK*03] SAUER F., SCHOEPF U. J., KHAMENE A., VOGT S., DAS M., SILVERMAN S. G.: Augmented reality system for ct-guided interventions: System description and initial phantom trials. In *Medical Imaging 2003* (2003), International Society for Optics and Photonics, pp. 384–394. 3

[TMS*06] TIETJEN C., MEYER B., SCHLECHTWEG S., PREIM B., HERTEL I., STRAUSS G.: Enhancing slice-based visualizations of medical volume data. In *EuroVis* (2006), vol. 6, pp. 123–130. 7

[UKLC10] UHERČÍK M., KYBIC J., LIEBGOTT H., CACHARD C.: Model fitting using ransac for surgical tool localization in 3-d ultrasound images. *IEEE Transactions on Biomedical Engineering 57*, 8 (2010), 1907–1916. 3

[VSG*04] VILLARD C., SOLER L., GANGI A., MUTTER D., MARESCAUX J.: Toward realistic radiofrequency ablation of hepatic tumors 3D simulation and planning. In *Medical Imaging 2004* (2004), International Society for Optics and Photonics, p. 586–595. 2

[WHP*09] WIDMANN G., HAIDU M., PALLWEIN L., KOVACS P., JASCHKE W., BALE R.: Stereotactic radiofrequency ablation: providing new dimensions in interventional oncology. In *World Congress on Medical Physics and Biomedical Engineering, September 7-12, 2009, Munich, Germany* (2009), Springer, pp. 83–86. 3

[WZD*05] WOOD B. J., ZHANG H., DURRANI A., GLOSSOP N., RANJAN S., LINDISCH D., LEVY E., BANOVAC F., BORGERT J., KRUEGER S., ET AL.: Navigation with electromagnetic tracking for interventional radiology procedures: a feasibility study. *Journal of vascular and interventional radiology 16*, 4 (2005), 493–505. 2